Soil Dynamics and Earthquake Engineering 117 (2019) 149–163

Contents lists available at ScienceDirect

Soil Dynamics and Earthquake Engineering

journal homepage: www.elsevier.com/locate/soildyn

A design method of viscoelastic damper parameters based on the elastic-plastic response reduction curve

Li Zhang[a], Mingzhou Su[a], Chao Zhang[b], Hua Shen[c], Md Mofakkharul Islam[c], Ruifu Zhang[c,*]

[a] Key Laboratory of Green Building in West China, Xi'an University of Architecture and Technology, Xi'an 710055, China
[b] College of Civil Engineering, Guangzhou University, Guangzhou 510006, China
[c] Research Institute of Structural Engineering and Disaster Reduction, Tongji University, Shanghai 200092, China

ARTICLE INFO

Keywords:
Viscoelastic damper
Design method
Elastic-plastic response reduction curve
Energy dissipation

ABSTRACT

The traditional design method of the elastic response reduction curve (ERRC) was used to design the parameters of the viscoelastic damper (VED), where the plastic behavior of the primary structure is neglected. Considering the structural plastic behavior, in this study, a direct design method is proposed to obtain the parameters of VEDs based on the elastic-plastic response reduction curve (EPRRC), which can illustrate the relationship between damper parameters and the response reduction effect in the elastic-plastic stage. First, the ERRC is developed to the EPRRC, and the differences between them are compared using the displacement and acceleration response difference ratios, which demonstrate an overestimated response reduction effect of VEDs in the elastic-plastic stage using the ERRC. Then, the corresponding design procedures are given based on the EPRRC by referring to the direct displacement-based design theory. Finally, a benchmark model is used to illustrate the effectiveness of this proposed design method by conducting a time history analysis. The analysis results indicate that the target story drift of the structure can be satisfied under different earthquake intensities using VEDs. Thus, based on this study, the development of the EPRRC can be considered worthwhile, and the proposed design method of VED parameters is easy to implement and is effective.

1. Introduction

Passive control systems using energy dissipation devices have been demonstrated to be effective for seismic damage mitigation of structures [1–4]. Four kinds of devices, friction dampers, metallic yield dampers, viscous dampers and viscoelastic dampers (VEDs), are often used. Among these devices [5–10], VEDs provide both supplemental damping and stiffness and show the characteristics of the phase angle difference of the force-displacement relationship, thus, in some ways, they are more difficult to apply in design and practical use than other devices.

A typical VED usually consists of flaky viscoelastic materials bonded with steel plates. When relative shear deformation takes place in the viscoelastic materials, the energy caused by dynamic loads is then dissipated. Due to effective energy dissipation capacity from low to high displacement [11], VEDs were used to reduce the structural vibration caused by different kinds of dynamic loads, such as winds, earthquakes and even human activities. The practical projects of VEDs in resisting wind-induced vibration began in the 1960s [12], and the application of VEDs for reducing the seismic responses of civil engineering structures began in the 1990s [13,14]. Recently, VEDs have been recommended to mitigate human-induced vibrations [15]. Additionally, for fire-damaged structures, VEDs are also applied for vibration control [16]. A number of experiments and theories have been improved by scholars such as Shen and Soong [17], Chang et al. [18], Tsai [19] and Xu et al. [20], who have demonstrated that the mechanical properties of VEDs strongly depend on temperature and frequency, thus complicating the analysis and design of structures with the addition of VEDs. Consequently, to effectively simulate the practical application of VEDs, classical rheological models and fractional derivative models are often suggested to describe the VEDs [21–26]. In the frequency domain, Lewandowski and Pawlak [21] combined the widely used response spectrum theory for structures mounted with fractional VEDs. In the time domain, using the generalized Maxwell model and Laguerre polynomial approximation technique, the computation time of dynamic analyses for structures with VEDs is clearly reduced [27]. Therefore, the reasonable model and appropriate theory have been recognized to be effective and feasible for the application of VEDs in practical engineering.

Aimed at the effective and convenient application of VEDs, a

* Corresponding author.
E-mail address: zhangruifu@tongji.edu.cn (R. Zhang).

https://doi.org/10.1016/j.soildyn.2018.09.050
Received 2 June 2018; Received in revised form 14 September 2018; Accepted 30 September 2018
Available online 06 December 2018

number of design methods for structures with VEDs have been presented with different standpoints. The traditional force-based design methods of VEDs use the force reduction factor and must often conduct iterative procedures based on linear static analysis [28]. However, force-based design methods neglect the lateral displacement of the structure, which is an important structural and nonstructural damage factor. To resolve this shortcoming, the direct displacement-based design method and the modified capacity spectrum method based on ATC-40 were presented for designing structures with VEDs [29–31]. These displacement-based design methods usually preset a target displacement to start the design procedure. Additionally, the process of accumulated energy dissipation is an important structural damage factor. Therefore, the energy-based design method was suggested by Habibi et al. [32] for structures with VEDs. Relying on the view of probability theory, reliability-based design methods were proposed by considering the stochastic seismic excitations and uncertain structural model parameters [33,34]. Furthermore, based on the optimization algorithms, some design methods of VEDs were presented. Zhang and Soong [35] suggested a sequential procedure based on the degree of controllability concept to determine the number and location of VEDs. However, identical dampers were used in all stories. Then, based on the study of Zhang and Soong [35], a step-by-step procedure was presented by Heydarinouri and Zahrai [36], and the dampers were distributed according to the lateral stiffness of each story. However, a time history analysis was needed at each sequence, which is time consuming. Singh and Moreschi [37] proposed a gradient-based algorithm to achieve the best performance by optimally distributing the dampers. By considering the variation in parameters for the structures with VEDs, Park et al. [38] suggested a genetic algorithm for the optimum design of a viscoelastically damped structural system. However, these methods are usually complex and not easy to implement.

The elastic response reduction curve (ERRC) presented by the Japan Society of Seismic Isolation (JSSI) [39] can reflect the relationships between the VED parameters and the response reduction effects. Because of its advantages of easy implementation and clear and graphical expression, the design method applied for VED parameters based on the ERRC has been accepted by many engineers. However, this method is limited by the elastic primary structure. Under strong ground motions, the primary structures may behave like plastic, and the structural behaviors in plastic stages are quiet different from the elastic stages. Therefore, it is necessary to take into account the plastic behavior of structures and develop the elastic-plastic response reduction curve (EPRRC).

In this paper, referring to the direct displacement-based design theory [30,40,41], a direct design method of viscoelastic dampers for damped structure based on the EPRRC is proposed. First, according to the design response spectrum and equivalent linear theory, the existing ERRC is developed to the EPRRC by considering the elastic-plastic behavior of the primary structure, which also has the advantages of the ERRC. Furthermore, the comparative study between the ERRC and EPRRC is illustrated using the displacement and acceleration response difference ratios. Then, by setting the target displacement and performing the pushover analysis, the corresponding design method is proposed, which does not require the time-consuming dynamic analysis process. Finally, this design method is applied to a benchmark model, and the time history analysis is conducted to illustrate the effectiveness of this method.

2. The development of the EPRRC

2.1. VED structural system characteristics

A single-degree-of-freedom (SDOF) mode with a VED, called the VED structural system, is used to illustrate the interactions among the VED, brace and primary structure, as shown in Fig. 1, where K_b and K_s are the elastic stiffness of the brace and primary structure, respectively;

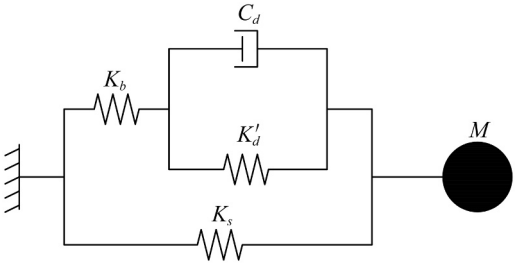

Fig. 1. VED structural system.

K'_d is the storage stiffness of VED, which is equal to the ratio of the damping force at the maximum displacement and the maximum displacement; and C_d is the damping coefficient. In this simplified model, the VED is modeled by a Kelvin element with a spring and dashpot connected in parallel, which is connected to the brace in series by the spring element in series, and then, the VED-brace component is incorporated into the primary structure in parallel.

Since the VEDs are mainly composed of a viscoelastic material that is usually velocity dependent, the values for VED parameters may be different under different load frequencies. Thus, in this paper, the relationships between the VED parameters below are determined under a certain frequency (usually the frequency of free vibration for the damped structure) [42]. Under harmonic excitation, the force-displacement relationships of VED, the VED-brace component and the VED structural system and their connections are illustrated in Fig. 2 [43], where the VED is assumed to be linear and idealized as an elliptical shape with a storage stiffness K'_d and K'_a stands for the storage stiffness of the VED-brace component. The total curve of the VED structural system can be calculated by adding the curves of the VED-brace component and primary structure, and K' is the storage stiffness of the VED structural system. Since the VED-brace component is composed of the VED and brace, which are connected in series, the force of the VED is equal to that of the VED-brace component, as well as only the brace. Then, the VED-brace component is connected to the primary structure in parallel, and the total system is called the VED structural system. The displacement of the VED-brace component is equal to that of the VED structural system as well as the primary structure. The maximum equality relationships of the damping force and displacement are shown in Fig. 2(a) and Fig. 2(b). The damping forces of the VED and VED-brace component at zero displacement are F_{d0} and F_{a0}, respectively, and F_b and u_b are the force and displacement of the brace, respectively. Furthermore, $u_{d,\max}$ and $u_{\max}$ are the maximum displacement of the VED and VED structural system, respectively.

Preliminarily, to estimate the energy absorbed by VED, the loss stiffness of the VED is defined as $K''_d = F_{d0}/u_{d,\max}$. Then, by considering that the VED and brace are acting in series and together constitute the VED-brace component, the storage stiffness K'_a and loss stiffness K''_a of the VED-brace component can be calculated as follows [44]:

$$K'_a = \frac{[(1+\eta_d^2)K'_d + K_b]K'_d K_b}{(K'_d + K_b)^2 + (\eta_d K'_d)^2} \tag{1}$$

$$K''_a = \frac{\eta_d K'_d K_b^2}{(K'_d + K_b)^2 + (\eta_d K'_d)^2} \tag{2}$$

where $\eta_d = K''_d/K'_d$ is the loss factor of VED. Similarly, the loss factor of the VED-brace component η_a can be obtained as:

$$\eta_a = K''_a K'_a = \frac{\eta_d}{1 + (1+\eta_d^2)K'_d/K_b} \tag{3}$$

By adding the stiffnesses K'_a and K_s, the storage stiffness of the VED structural system K' can be written as:

$$K' = K'_a + K_s \tag{4}$$

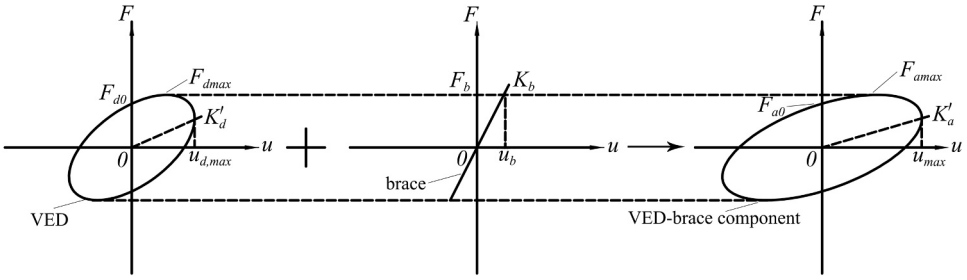

(a) Relationship between the VED and VED-brace component

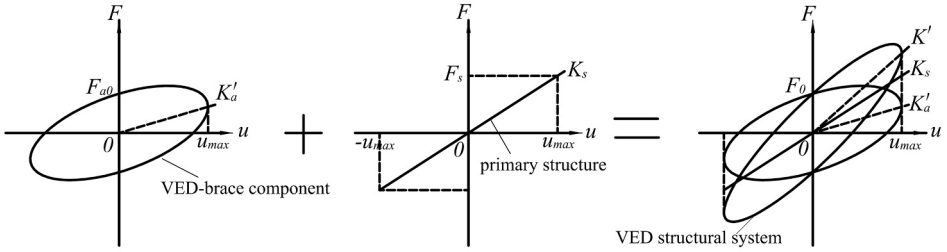

(b) Relationship between the VED-brace component and VED structural system

Fig. 2. Force-displacement relationships.

The maximum displacement and the force at zero displacement of the VED-brace component are assumed to be equal to that of the VED structural system. Thus, K_a'' and the loss stiffness of the VED structural system K'' are equal ($K_a'' = K''$). Now, the loss factor of the VED structural system η can be calculated as:

$$\eta = K''/K' = \frac{\eta_a}{1 + K_s/K'_a} \tag{5}$$

The relationship of $u_{d,\max}$ and $u_{\max}$ can be expressed as:

$$u_{\max} = \sqrt{K_d''/K_a''}\, u_{d,\max} \tag{6}$$

2.2. Response reduction theory

Plotting the response spectrum parameters of the VED structural system with the design response spectrum, the response reduction theory can be derived. By providing added damping and stiffness, supplemental VEDs increase the damping ratio and decrease the period of the primary structure. Consequently, dynamic responses are mitigated according to the seismic design response spectrum theory. The spectral displacement S_d, spectral pseudovelocity S_{pv} and spectral pseudoacceleration S_{pa} are three primary parameters of the response spectrum theory. The relationships between them can be expressed as follows [45]:

$$S_d\left(T, \zeta\right) = \frac{T}{2\pi} S_{pv}\left(T, \zeta\right) = \left(\frac{T}{2\pi}\right)^2 S_{pa}\left(T, \zeta\right) \tag{7}$$

where T is the structure natural vibration period, and ζ is the damping ratio.

According to the theory and equation mentioned above, the equivalent period T_{eq} as well as the equivalent damping ratio ζ_{eq} of the VED structural system are suggested to estimate the reduced seismic responses. The equivalent period T_{eq} can be calculated as:

$$T_{eq} = T_s\sqrt{\frac{K_s}{K'}} = T_s\sqrt{\frac{K_s}{K_s + K'_a}} \tag{8}$$

where T_s is the natural vibration period of the primary structure.

The equivalent damping ratio of the VED structural system ζ_{eq} can be determined as:

$$\zeta_{eq} = \zeta_0 + \varphi\zeta_a \tag{9}$$

where the recommended value of $\varphi = 0.92$ by JSSI [39] is called the reduction factor caused by the seismic response of random vibration and the phase angle difference in the VED structural system, ζ_0 is the material damping ratio, and ζ_a is the added damping ratio of the VED. Using the energy dissipation method, ζ_a can be calculated as follows:

$$\zeta_a = \frac{E_d}{4\pi E_s} = \frac{\eta}{2} \tag{10}$$

where $E_d = \pi K'' u_{\max}^2$ is the energy dissipated by the VED structural system and $E_s = (K_s + K'_a)u_{\max}^2/2$ is the strain energy of the VED structural system.

As mentioned above, the addition of VEDs can effectively mitigate the seismic responses of the primary structure; thus, to measure the reduction effect, the displacement reduction ratio R_d and pseudoacceleration reduction ratio R_{pa} are defined as follows [44]:

$$R_d = \frac{S_d(T_{eq}, \zeta_{eq})}{S_d(T_s, \zeta_0)} = D_\zeta \frac{T_{eq}}{T_s}\frac{S_{pv}(T_{eq}, \zeta_0)}{S_{pv}(T_s, \zeta_0)} \tag{11}$$

$$R_{pa} = \frac{S_{pa}(T_{eq}, \zeta_{eq})}{S_{pa}(T_s, \zeta_0)} = D_\zeta \frac{T_s}{T_{eq}}\frac{S_{pv}(T_{eq}, \zeta_0)}{S_{pv}(T_s, \zeta_0)} \tag{12}$$

$$D_\zeta = \sqrt{\frac{1 + 25\zeta_0}{1 + 25\zeta_{eq}}} \tag{13}$$

where D_ζ is the reduction rate of the design response spectrum caused by the increasing damping ratio. Because of the phase angle of the force-displacement relationship of the VED structural system, the spectral acceleration $S_a(T_{eq}, \zeta_{eq})$ of the VED structural system differs with the pseudoacceleration $S_{pa}(T_{eq}, \zeta_{eq})$ of the VED structural system [45]. Their numerical relationship is derived from Fu and Kasai [43], which can be expressed as:

$$S_a\left(T_{eq}, \zeta_{eq}\right) = \sqrt{1 + 4\zeta_{eq}^2}\, S_{pa}\left(T_{eq}, \zeta_{eq}\right) \tag{14}$$

Then, the acceleration reduction ratio R_a can be written as:

$$R_a = \frac{S_a(T_{eq}, \zeta_{eq})}{S_a(T_s, \zeta_o)} = \sqrt{1 + 4\zeta_{eq}^2}\frac{S_{pa}(T_{eq}, \zeta_{eq})}{S_{pa}(T_s, \zeta_o)} = \sqrt{1 + 4\zeta_{eq}^2}R_{pa} \tag{15}$$

For different natural vibration periods of the structures, the characteristics of S_{pv} and S_{pa} are different. Then, the formulae of R_d and R_a can be further derived as follows:

(1) When the natural vibration periods of the structures are in the short period range, S_{pa} is a constant, and S_{pv} is directly proportional to T. Additionally, the equivalent period is almost unchanged under random earthquake excitation. Therefore, the Eqs. (11) and (12) can be written as:

$$R_d = D_\zeta\left(\frac{T_{eq}}{T_s}\right)^2 \tag{16}$$

$$R_{pa} = R_d\left(\frac{T_s}{T_{eq}}\right)^2 \tag{17}$$

Substituting Eq. (17) into Eq. (15), R_a can be written as:

$$R_a = \sqrt{1 + 4\zeta_{eq}^2}R_{pa} = \sqrt{1 + 4\zeta_{eq}^2}R_d\left(\frac{T_s}{T_{eq}}\right)^2 \tag{18}$$

(2) When the natural vibration periods of structures are in the medium or long period range, S_{pv} is a constant. Then, Eq. (11) can be simplified as:

$$R_d = D_\zeta\frac{T_{eq}}{T_s} \tag{19}$$

The calculation for R_a is the same as Eq. (18).

2.3. The details of the ERRC

According to the aforementioned formulae, the response reduction ratios R_d and R_a can be written as a continuous function of η_d and K''_d/K_s by substituting Eqs. (8) and (13) into the equations of R_d and R_a. Then, the R_d-R_a curve, the so-called ERRC, can be plotted. The detailed drawing procedure will be illustrated subsequently.

In this paper, the ERRC has been plotted according to Chinese code [46], and the formula for the spectral reduction rate D_ζ caused by increasing damping ratio mentioned earlier and the expression for the design response spectrum determined below from Eqs. (20)–(23) have been developed accordingly. According to the code, the range from the short to the medium period are recommended between 0.1 s and 5 T_g, which is the period range of most practical buildings, where T_g is the characteristic period of the design response spectrum considering the impact of near and far field earthquakes. Especially, further investigation may be needed for the damped structure under the near field earthquakes due to the characteristic of short duration pulses of long period with large peak ground velocities and accelerations. The design response spectrum can be expressed as:

$$S_{pa} = \begin{cases} [10(\eta_2 - 0.45)T + 0.45]\alpha_{\max}g, & (0<T \le 0.1s) \\ \eta_2\alpha_{\max}g, & (0.1s < T \le T_g) \\ \left(\frac{T_g}{T}\right)^\gamma\eta_2\alpha_{\max}g, & (T_g<T \le 5T_g) \\ [\eta_2 0.2^\gamma - \eta_1(T - 5T_g)]\alpha_{\max}g, & (5T_g < T \le 6s) \end{cases} \tag{20}$$

$$\gamma = 0.9 + \frac{0.05 - \zeta}{0.3 + 6\zeta} \tag{21}$$

$$\eta_1 = 0.02 + \frac{0.05 - \zeta}{4 + 32\zeta} \tag{22}$$

$$\eta_2 = 1 + \frac{0.05 - \zeta}{0.08 + 1.6\zeta} \tag{23}$$

where $\alpha_{\max}$ is the maximum of the earthquake affecting coefficient, g is the acceleration of gravity, γ is the exponential of the downward section of the curve, η_1 is the slope adjustment coefficient of the linear descending section, and η_2 is the damping adjustment factor.

According to the derived response reduction ratio Eq. (11) and the characteristics of S_{pv}, R_d can be expressed as follows using the design response spectrum given above:

(1) For short period structures ($0.1s < T \le T_g$), R_d can be derived as

$$R_d = \frac{S_d(T_{eq}, \zeta_{eq})}{S_d(T_s, \zeta_0)} = \frac{\eta_{2eq}}{\eta_{20}}\left(\frac{T_{eq}}{T_s}\right)^2 \tag{24}$$

where η_{2eq} and η_{20} can be calculated from Eq. (23) using the value of ζ_{eq} and ζ_0, respectively.

(2) For medium period structures ($T_g < T \le 5T_g$), R_d can be derived as

$$R_d = \frac{S_d(T_{eq}, \zeta_{eq})}{S_d(T_s, \zeta_0)} = \frac{\eta_{2eq}}{\eta_{20}}\left(\frac{T_{eq}}{T_s}\right)^{2-\gamma_{eq}}\left(\frac{T_s}{T_g}\right)^{\gamma_0-\gamma_{eq}} \tag{25}$$

where γ_{eq} and γ_0 can be calculated from Eq. (21) using the value of ζ_{eq} and ζ_0, respectively.

By expressing stiffness ratios which are the ratio of stiffness parameters to K_s (i.e., K_b/K_s and K''_d/K_s etc.), the ERRC can be plotted by the following procedures:

1. Assume a reasonable stiffness ratio of the brace to primary structure K_b/K_s, which is usually a quite large value, and the recommended value is $K_b/K_s > 5$ [43].
2. Set the values of η_d and K''_d/K_s, and then calculate the ratio of equivalent period T_{eq}/T_s and equivalent damping ratio ζ_{eq} according to Eqs. (8) and (9), respectively.
3. Calculate the response spectrum reduction rate η_{2eq}/η_{20} using the values of ζ_0 and ζ_{eq} (short and medium period). For the medium period primary structure, the values of γ_0 and γ_{eq} should be calculated, and the ratio T_s/T_g should be set.
4. For short period structures, calculate R_d using Eq. (24); for the medium period, calculate R_d using Eq. (25). R_a can be calculated using Eq. (18).
5. Next, repeat steps 2–4 illustrated above; the ERRCs can be plotted according to different η_d and K''_d/K_s.

For an RC structure, ζ_0 is equal to 0.05. As shown in Fig. 3, by setting $K_b/K_s = 10$, $0.3 \le \eta_d \le 2$, $0 \le K''_d/K_s \le 3$, and $T_s/T_g = 1.5$, the ERRCs can be plotted for structures of short and medium periods, respectively.

For the short period structure, both reduction ratios R_d and R_a are less than 1, which means the structural responses are reduced using different combinations of η_d and K''_d/K_s. With a small constant K''_d/K_s, as factor η_d increases, the reduction ratio R_a decreases. However, for a relatively large constant K''_d/K_s, such as $K''_d/K_s = 3$, the reduction ratio R_a decreases until a specific increasing value of η_d, and then, R_a starts to increase. Thus, the combination of a large constant K''_d/K_s and specific large η_d value of the VED cannot reduce the acceleration response continuously.

For a medium period structure with a constant η_d and increasing stiffness ratio K''_d/K_s, the reduction ratio R_a decreases initially until some specific values of K''_d/K_s, and then, it starts to increase, whereas R_d decreases continuously. Additionally, the combination of relatively large K''_d/K_s value and a small η_d value may lead to a R_a value that is larger than 1. Thus, this combination is unreasonable for acceleration response reduction.

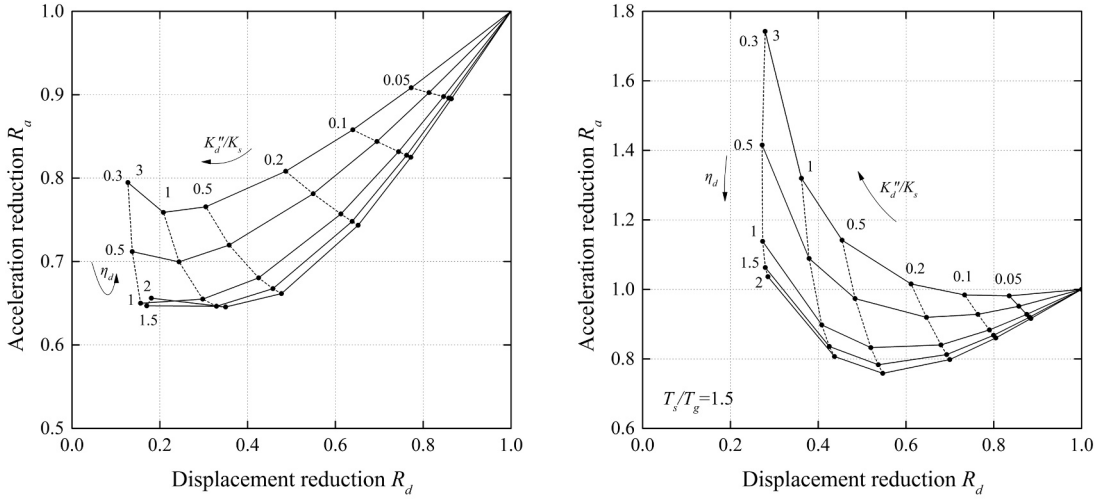

Fig. 3. ERRCs.

2.4. The details of the EPRRC

In this section, the ERRC is developed to the EPRRC. The plastic performance of the primary structures is taken into account. Because under moderate and severe earthquakes, the primary structures with VEDs produce the larger drift compared with frequent earthquakes, which causes the primary structure to enter a plastic stage. According to the philosophy of the performance-based design method, the performance targets should be satisfied not only in the elastic stage but also in the plastic stage of the structures under different earthquake levels. Obviously, when the structures are in the plastic stage, the design method based on the ERRC cannot ensure that the performance targets are satisfied. Therefore, the development of the EPRRC is worthwhile and can be reasonably used to estimate and design structures with VEDs in the elastic-plastic stage.

To derive the EPRRC, the primary structure is considered with an elastic-plastic bilinear curve, and the VED-brace component is still modeled with an elliptical shape. By superposing these two curves, the elastic-plastic curve of the VED structural system can be depicted as shown in Fig. 4, where F_{sy} and u_{sy} are the yielding force and yielding displacement of the primary structure, respectively, β is the stiffness loss ratio after yielding, and K'_s and K_{eq} are the secant stiffness of the primary structure and elastic-plastic VED structural system, respectively.

Similar to the ERRC, the equivalent period T'_{eq} and the equivalent damping ratio ζ'_{eq} of the elastic-plastic VED structural system need to be calculated to derive the equations for the EPRRC. For the elastic-plastic primary structure, the equivalent period of primary structure T'_s can be calculated as:

$$T'_s = T_s\sqrt{\frac{K_s}{K'_s}} = T_s\sqrt{\frac{\mu_s}{1+\beta\mu_s-\beta}} \tag{26}$$

where $\mu_s = u_{\max}/u_{sy}$ is the plasticity factor. Then, T'_{eq} can be expressed as:

$$T'_{eq} = T'_s\sqrt{\frac{K'_s}{K_{eq}}} = T'_s\sqrt{\frac{1+\beta(\mu_s-1)}{1+\beta(\mu_s-1)+\mu_s K'_a/K_s}} \tag{27}$$

To calculate the equivalent damping ratio ζ'_{eq}, in addition to the material damping ratio ζ_0 and the added damping ratio of the VED ζ'_a, the effective damping ratio of the primary structure ζ'_s should also be considered. Then, ζ'_{eq} can be calculated as:

$$\zeta'_{eq} = \zeta_0 + \zeta'_s + \varphi\zeta'_a \tag{28}$$

By using the similar expression of Eq. (10), the two terms of Eq. (28) ζ'_a and ζ'_s can be derived as follows:

$$\zeta'_a = \frac{1}{2}\frac{\mu_s K''_a/K_s}{1+\beta(\mu_s-1)+\mu_s K'_a/K_s} \tag{29}$$

$$\zeta'_s = \frac{2\kappa(1-\beta)(\mu_s-1)}{\pi\mu_s[1+\beta(\mu_s-1)+\mu_s K'_a/K_s]} \tag{30}$$

where κ is the damping modification coefficient in which the feature of the hysteretic loop is taken into account. For the full, moderate and poor hysteretic loops, it is recommended by ATC-40 that the values of κ are 1, 2/3 and 1/3, respectively [31]. The detailed derivation process of ζ'_s and ζ'_a can be found in Appendix A.

Considering the randomness of earthquake intensity, the plasticity factor will change from 1 to μ_s. Accordingly, ζ'_s will also change with the change in μ_s. Therefore, under random seismic excitation, ζ'_s can be expressed as:

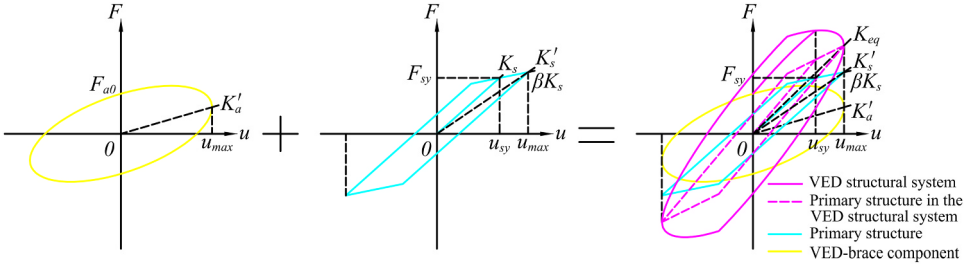

Fig. 4. Force-displacement relationship of the VED structural system.

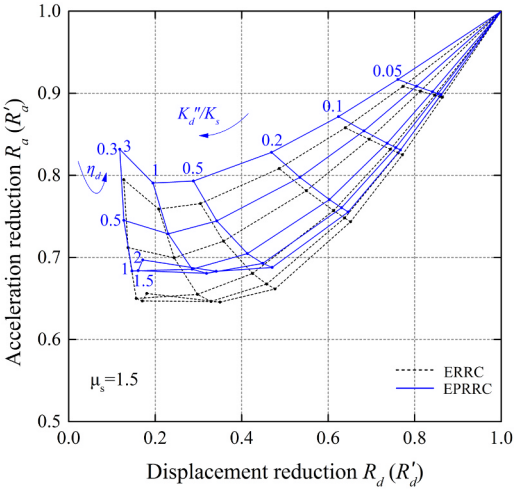

(a) Short period structures ($\mu_s = 1.5$)

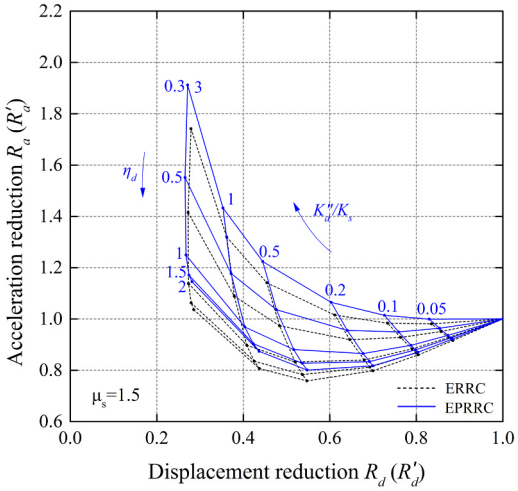

(b) Medium period structures ($\mu_s = 1.5$)

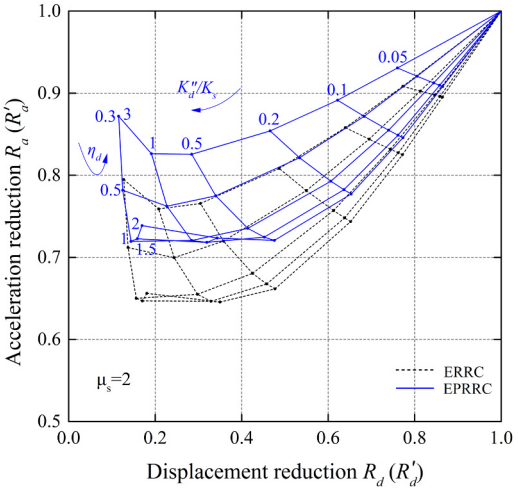

(c) Short period structures ($\mu_s = 2$)

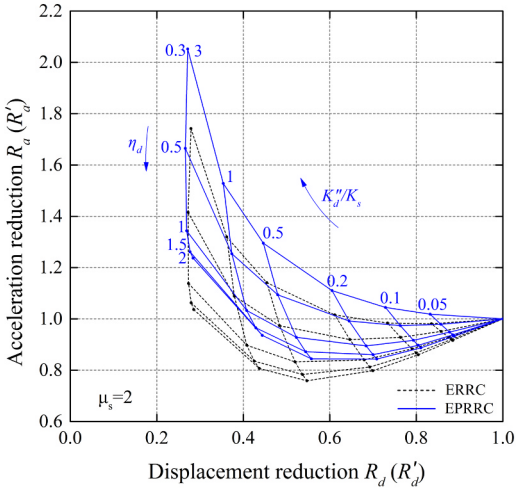

(d) Medium period structures ($\mu_s = 2$)

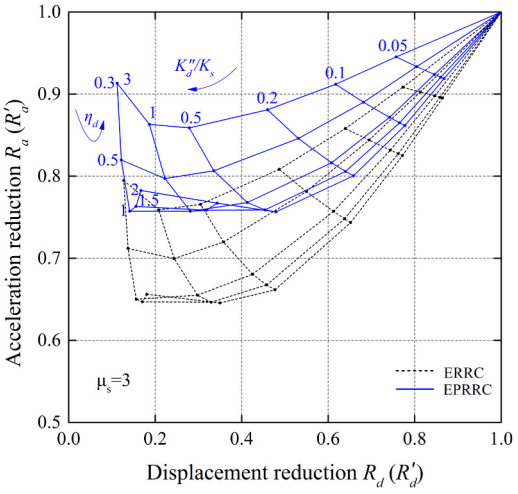

(e) Short period structures ($\mu_s = 3$)

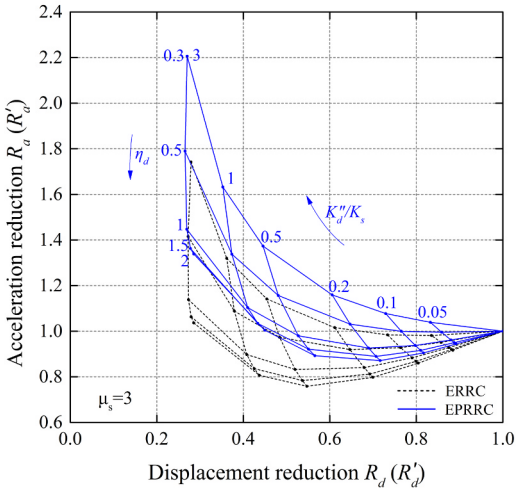

(f) Medium period structures ($\mu_s = 3$)

Fig. 5. ERRCs and EPRRCs.

$$\zeta_s' = \frac{1}{\mu_s}\int_1^{\mu_s} \zeta_s'(\mu)\, d\mu = \frac{2\kappa}{\pi\mu_s}\left\{\ln\frac{[m(\mu_s-1)+n]^{\frac{n}{m}}}{\mu_s} - \frac{n}{m}\ln n\right\} \tag{31}$$

$$m = \beta + K_a'/K_s \tag{32}$$

$$n = 1 + K'_a/K_s \tag{33}$$

Due to the plastic behavior of the primary structure, the spectral displacement S_d and acceleration S_a must be calculated to derive the response ratios for the elastic-plastic primary structure. Therefore, the equivalent damping ratio of the primary structure without VED ζ_{eq}^* should be derived. Considering ζ_0, ζ_{eq}^* can be calculated as:

$$\zeta_{eq}^* = \zeta_0 + \zeta_s^* \tag{34}$$

where ζ_s^* is the effective damping ratio of the elastic-plastic primary structure without VED. Using a similar expression as Eq. (10), ζ_s^* can be derived as:

$$\zeta_s^* = \frac{2\kappa(1-\beta)(\mu_s-1)}{\pi\mu_s(1+\beta\mu_s-\beta)} \tag{35}$$

The detailed derivation process of ζ_s^* can also be found in Appendix A.

Similar to the derivation of ζ_s', due to the random seismic excitation, ζ_s^* can be derived as:

$$\zeta_s^* = \frac{1}{\mu_s}\int_1^{\mu_s} \zeta_s^*(\mu)\, d\mu = \frac{2\kappa}{\pi\beta\mu_s}\ln\frac{1+\beta\mu_s-\beta}{\mu_s^{\beta}} \tag{36}$$

Then, according to the natural vibration periods of the primary structures, the elastic-plastic response reduction ratios R_d' and R_a' for displacement and acceleration, respectively, can be defined as follows:

(1) For short period structures ($0.1s < T \le T_g$), R_d' can be derived as

$$R_d' = \frac{S_d(T_{eq}', \zeta'_{eq})}{S_d\left(T_s', \zeta_{eq}^*\right)} = \frac{\eta'_{2eq}}{\eta_{2s}}\left(\frac{T'_{eq}}{T_s'}\right)^2 \tag{37}$$

where η'_{2eq} and η_{2s} can be calculated from Eq. (23) using the values of ζ'_{eq} and ζ_{eq}^*, respectively. Similar to the derivation of R_a, due to the phase angle of the force-displacement relationship of the VED structural system, R_a' can be written as:

$$R_a' = \sqrt{1+4\zeta'^2_{eq}}R_{pa}' = \sqrt{1+4\zeta'^2_{eq}}R'_d\left(\frac{T_s'}{T'_{eq}}\right)^2 \tag{38}$$

(2) For the medium period structures ($T_g < T \le 5T_g$), R'_d can be derived as

$$R'_d = \frac{S_d\left(T'_{eq}, \zeta'_{eq}\right)}{S_d\left(T_s', \zeta_{eq}^*\right)} = \frac{\eta'_{2eq}}{\eta_{2s}}\left(\frac{T'_{eq}}{T_s'}\right)^{2-\gamma'_{eq}}\left(\frac{T_s'}{T_g}\right)^{\gamma_s-\gamma'_{eq}} \tag{39}$$

$$R'_d = \frac{S_d\left(T'_{eq}, \zeta'_{eq}\right)}{S_d\left(T_s', \zeta_{eq}^*\right)} = \frac{\eta'_{2eq}}{\eta_{2s}}\left(\frac{T'_{eq}}{T_s'}\right)^{2-\gamma'_{eq}}\left(\frac{T_s'}{T_g}\right)^{\gamma_s-\gamma'_{eq}}$$ (39)

where γ'_{eq} and γ_s can be calculated from Eq. (21) using the values of ζ'_{eq} and ζ_{eq}^*, respectively. The calculation of R'_a is the same as Eq. (38).

According to the abovementioned formulae, the response reduction ratios R'_d and R'_a can also be written as a continuous function of η_d and K_d''/K_s. Then, by referring to the plotting procedures of the ERRC, the $R'_d - R'_a$ curve, which is called the EPRRC, can be plotted similarly. As mentioned, the VED parameters are usually frequency dependent. Therefore, under different excitation frequencies, the response reduction ratios R_a' and R_a' are usually different for the change in VED parameters. The EPRRCs comprise the set of the response reduction ratio point (R_a', R_a'). For a target primary structure, the EPRRCs can only be plotted according to the analysis result and the design response spectrum.

2.5. Comparative study between the EPRRC and ERRC

To analyze the influence of the plastic behavior of the primary structures on the response reduction of the VED structural system, the EPRRC and ERRC are drawn together with the same parameters of the VEDs. To identify the differences between them, different plasticity coefficients of the primary structure $\mu_s = 1.5$, 2.0 and 3.0, are considered, $\beta = 0.6$, $\kappa = 2/3$ are assumed, and the parameters of VEDs are set as $K_b/K_s = 10$, $\zeta_0 = 0.05$, $T_s/T_g = 1.5$, $0.3 \le \eta_d \le 2$ and $0 \le K_d''/K_s \le 3$, equivalent to the parameters in Fig. 3. The ERRCs and the EPRRCs are then plotted together in Fig. 5. Based on a rough observation, the tendency of the EPRRCs is similar to that of the ERRCs, but the differences between the ERRCs and the EPRRCs are also obvious. To measure the differences, ρ_d and ρ_a are two difference ratios of the displacement reduction and the acceleration reduction for structures with different periods, respectively, as shown in Tables 1–4.

Based on the same value of η_d or K_d''/K_s, the difference ratios in response reduction for different plasticity coefficients of the elastic-plastic primary structure are compared, as shown in Tables 1–4. For example, for short period structures in Table 1, with the same plasticity coefficient, for $\eta_d = 1$, as K_d''/K_s increases, ρ_d decreases as negative values, and ρ_a increases as positive values. Thus, the ERRC may underestimate the displacement response reduction and overestimate the acceleration response reduction, especially for a large K''_d/K_s. Then, for $\eta_d = 1$, with an increasing μ_s, ρ_d increases with small values of K''_d/K_s but decreases with large values of K_d''/K_s, and ρ_a increases continuously with the same values of K_d''/K_s. In Table 2, with the same plasticity coefficient, for $K_d''/K_s = 0.5$, the difference ratios ρ_d and ρ_a are increasing continuously with an increasing η_d, where ρ_a always has a positive value and ρ_d usually has a negative value, except for the condition of $\mu_s = 3$, $\eta_d = 2$. This finding indicates that with a large combination of μ_s and η_d, ERRC shows a tendency toward an overestimation of the displacement response reduction. For $K_d''/K_s = 0.5$, with an increasing μ_s, ρ_d decreases with the small values of η_d but increases with large values of η_d, and ρ_a increases continuously with same values of η_d. Similarly, these increasing and decreasing regularities can also be found for medium period structures, as shown in Tables 3–4. Positive values of ρ_d are found to be greater than those in short period structures, especially for a large μ_s. Thus, the ERRC may overestimate the displacement response reduction due to the development of plastic behavior for the medium period structure. Similarly, for other values of η_d and K_d''/K_s, this comparison can also be performed as described above.

Because of the development of the elastic-plastic behavior of the primary structures, according to the comparative results mentioned above, the ERRC may overestimate the response reduction effects of the

Table 1
Difference ratios for short period structures ($\eta_d = 1$).

Difference ratios	$\rho_d = \frac{R_d'-R_d}{R_d}\times 100\%$			$\rho_a = \frac{R_a'-R_a}{R_a}\times 100\%$		
μ_s	1.5	2	3	1.5	2	3
K_d''/K_s 0.05	−0.63%	−0.31%	−0.11%	0.46%	1.64%	2.90%
0.1	−1.02%	−0.55%	−0.27%	0.88%	2.78%	4.79%
0.2	−1.58%	−1.04%	−0.80%	1.77%	4.71%	7.81%
0.5	−2.78%	−2.55%	−2.82%	3.56%	8.06%	12.84%
1	−4.12%	−4.51%	−5.48%	4.69%	9.99%	15.59%
3	−6.25%	−7.66%	−9.72%	5.15%	10.70%	16.49%

Table 2
Difference ratios for short period structures ($K''_d/K_s = 0.5$).

Difference ratios	$\rho_d = \frac{R'_d - R_d}{R_d} \times 100\%$			$\rho_a = \frac{R'_a - R_a}{R_a} \times 100\%$		
μ_s	1.5	2	3	1.5	2	3
η_d 0.3	−5.37%	−6.65%	−8.52%	3.59%	7.82%	12.17%
0.5	−4.34%	−5.04%	−6.30%	3.43%	7.66%	12.05%
1	−2.78%	−2.55%	−2.82%	3.56%	8.06%	12.84%
1.5	−1.93%	−1.17%	−0.84%	3.78%	8.54%	13.67%
2	−1.39%	−0.29%	0.44%	3.97%	8.93%	14.34%

Table 3
Difference ratios for medium period structures ($\eta_d = 1$).

Difference ratios	$\rho_d = \frac{R'_d - R_d}{R_d} \times 100\%$			$\rho_a = \frac{R'_a - R_a}{R_a} \times 100\%$		
μ_s	1.5	2	3	1.5	2	3
K''_d/K_s 0.05	−0.22%	0.22%	0.57%	0.87%	2.18%	3.60%
0.1	−0.30%	0.41%	0.99%	1.62%	3.78%	6.11%
0.2	−0.38%	0.63%	1.43%	3.01%	6.47%	10.24%
0.5	−0.65%	0.55%	1.41%	5.83%	11.51%	17.74%
1	−1.14%	−0.09%	0.53%	7.94%	15.07%	22.94%
3	−2.13%	−1.55%	−1.46%	9.77%	18.03%	27.13%

Table 4
Difference ratios for medium period structures ($K''_d/K_s = 0.5$).

Difference ratios	$\rho_d = \frac{R'_d - R_d}{R_d} \times 100\%$			$\rho_a = \frac{R'_a - R_a}{R_a} \times 100\%$		
μ_s	1.5	2	3	1.5	2	3
η_d 0.3	−2.05%	−1.75%	−1.90%	7.22%	13.47%	20.29%
0.5	−1.51%	−0.88%	−0.65%	6.48%	12.38%	18.81%
1	−0.65%	0.55%	1.41%	5.83%	11.51%	17.74%
1.5	−0.16%	1.37%	2.61%	5.65%	11.33%	17.62%
2	0.15%	1.89%	3.38%	5.60%	11.32%	17.68%

VED, especially for the acceleration response reduction effects. Therefore, it is unreasonable to use the ERRC to estimate the response reduction effects for the elastic-plastic VED structural system, and it is necessary to develop the EPRRC and suggest the corresponding design method of the VED parameters.

3. Design of the VED parameters

Based on the EPRRC, the step-by-step procedures for describing the design method are provided below, and a corresponding flowchart is shown in Fig. 6.

1. Conduct a pushover analysis on the elastic-plastic primary structure denoted as S0, and determine the story shear force Q_i and story drift δ_i. Then, calculate the story elastic stiffness K_{si}, and generate the capacity spectrum $S_a - S_d$.
2. Obtain the structural performance point (SPP) (S_{du}, S_{au}) using the capacity spectrum method, and determine the drift distribution δ_i of each story at the pushover analysis step of the SPP.
3. Set the target drift $[\delta]$, calculate the displacement reduction ratio of the ith story R'_{di} using Eq. (40) below, and then choose the stories at which R'_{di} is less than 1 to install the VEDs [40].

$$R'_{di} = \frac{[\delta]}{\delta_i} \tag{40}$$

4. Plot the area equivalent bilinear capacity spectrum that intersects with the capacity spectrum at the SPP in the plastic stage, and then, the inflection point can be denoted as the yielding point (S_{dy}, S_{ay}). Calculate the plasticity coefficient μ_s and the ratio of the post-yielding stiffness β using the following equations:

$$\mu_s = \frac{S_{du} S_{ay}}{S_{dy} S_{au}} \tag{41}$$

$$\beta = \frac{S_{dy}(S_{au} - S_{ay})}{S_{ay}(S_{du} - S_{dy})} \tag{42}$$

5. Set the stiffness ratio K_b/K_s and then plot the EPRRCs. Assume the loss factor η_{di} (the typical value is 1–1.4, which is close to the bottom of the figure of the EPRRC) of the VEDs installed at the ith story, and obtain the ratio of the stiffness K''_{di}/K_{si} according to the EPRRCs and R'_{di}. Moreover, the condition $K_{bi}/K''_{di} > 5$ should be fulfilled [43].
6. Calculate the storage stiffness of the VEDs $K'_{di} = K''_{di}/\eta_{di}$ and the brace stiffness K_{bi}. The maximum damping force F_{di} can then be expressed as follows:

$$F_{di} = \sqrt{1 + \eta_{di}^2} K'_{di} h_i [\delta] \sqrt{\frac{K''_{ai}}{K''_{di}}} \tag{43}$$

where K''_{ai} can be calculated according to Eq. (2).
7. Choose the suitable VEDs and braces installed at the ith story.

4. Design example and verification

The proposed design method is illustrated by application to a benchmark six-story RC structure to design the parameters of VEDs for mitigating the seismic responses [47]. The six-story RC structure model is built by the program PERFORM-3D [48]. Then, a time history analysis is conducted to verify the effectiveness of the design procedures suggested above.

4.1. Model illustration of the structure

In this study, a benchmark six-story RC frame is denoted S0. The plan, elevation, and corresponding story weight are shown in Fig. 7. The cross dimensions of the structural members are listed in Table 5. The design response spectrum for moderate earthquakes provided by Chinese code is given as follows:

$$S_{pa} = \begin{cases} 1 + 11.5T, & (0 < T \le 0.1s) \\ 2.25, & (0.1s < T \le 0.4s) \\ 2.25\left(\frac{0.4}{T}\right)^{0.9}, & (0.4s < T \le 2s) \\ 2.25[0.2^{0.9} - 0.02(T - 2)], & (2s < T \le 6s) \end{cases} \tag{44}$$

The recurrence time-interval of the moderate earthquake is 475 years. For this structure, ζ_0 is set to 0.05.

For the longitudinal steel bars, the yielding strengths and ultimate strengths are 400 MPa and 520 MPa, respectively. For the stirrup steel bars, the yielding strengths and ultimate strengths are 235 MPa and 352.5 MPa, respectively. The axial compressive strength of the concrete is 30 MPa. Further details for the concrete are illustrated in Chinese code for design of concrete structures [49]. The strut model is used to model this frame structure. On each side of the beams and columns, the moment hinges and fiber segments are used to simulate the plastic deformation of the structural members, respectively. The moment-curvature relationship of the moment hinges is based on the trilinear model recommended by Takeda [50]. The fiber segments are built according to the placement of the steel bar in the columns.

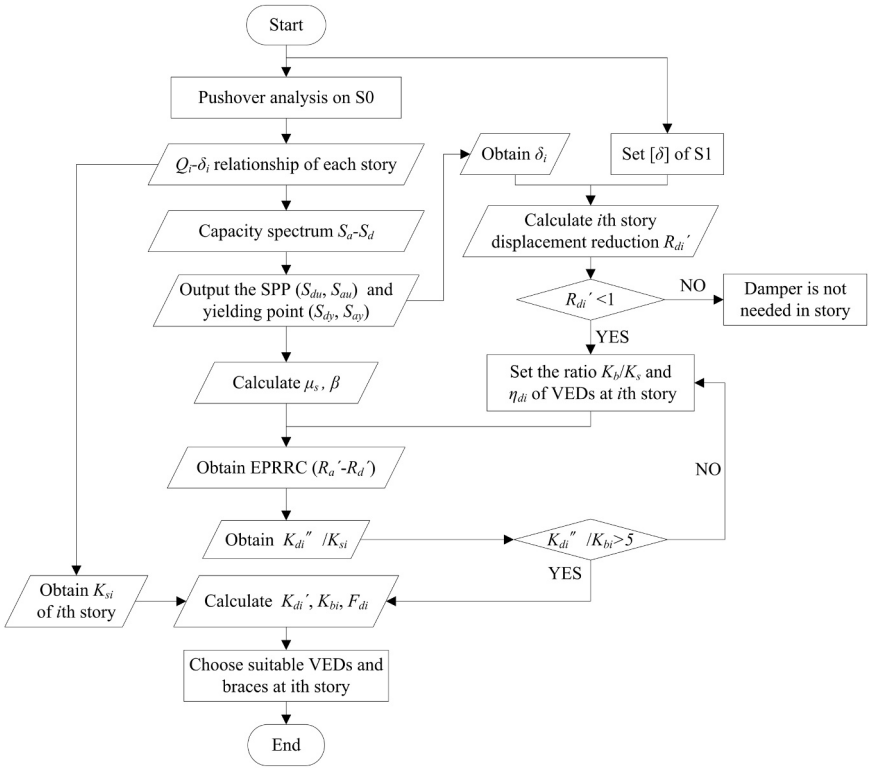

Fig. 6. Flowchart of the design procedure.

4.2. Design result

In this study, the target drift [δ] for S0 is set to 1/200. Pushover analysis is performed on S0. Then, the capacity spectrum can be obtained as shown in Fig. 8. According to the capacity spectrum method, the SPP is determined to be (66.5 mm, 94.4 gal). The story elastic stiffness can be calculated according to the $Q_i - \delta_i$ relationship of each story. At the pushover analysis step of the SPP, the story shear force Q_i and the story drift δ_i can be gathered. Then, the displacement reduction ratio R_{di}' is calculated using Eq. (40). These results are listed in Table 6. According to the condition $R_{di}' < 1$ illustrated in the design procedure, stories 1, 2 and 3 should be installed with VEDs to mitigate the seismic response.

Assuming that the area under the equivalent bilinear capacity spectrum is equal to that of the capacity spectrum, the equivalent bilinear capacity spectrum can be obtained by intersecting the capacity spectrum at the SPP, and the yielding point can be determined at the inflection point as (36.0 mm, 62.0 gal), as shown in Fig. 8. Then, the plasticity coefficient μ_s and stiffness loss ratio after yielding β can be calculated as 1.21 and 0.62 using Eqs. (41) and (42), respectively.

The natural vibration period is obtained as 1.51 s by performing the model analysis, which is in the medium period range. T_s/T_g is calculated as 3.78. Then, the EPRRC is plotted for the medium period structure by

Table 5
Dimensions of structural members.

Story	Cross dimension of beam (mm × mm)			Cross dimension of column (mm × mm)	Slab thickness (mm)
	X1–X8		Y1–Y4		
	Side span	Middle span			
1	300 × 600	300 × 400	300 × 400	450 × 450	120
2–6	300 × 600	300 × 400	300 × 400	400 × 400	120

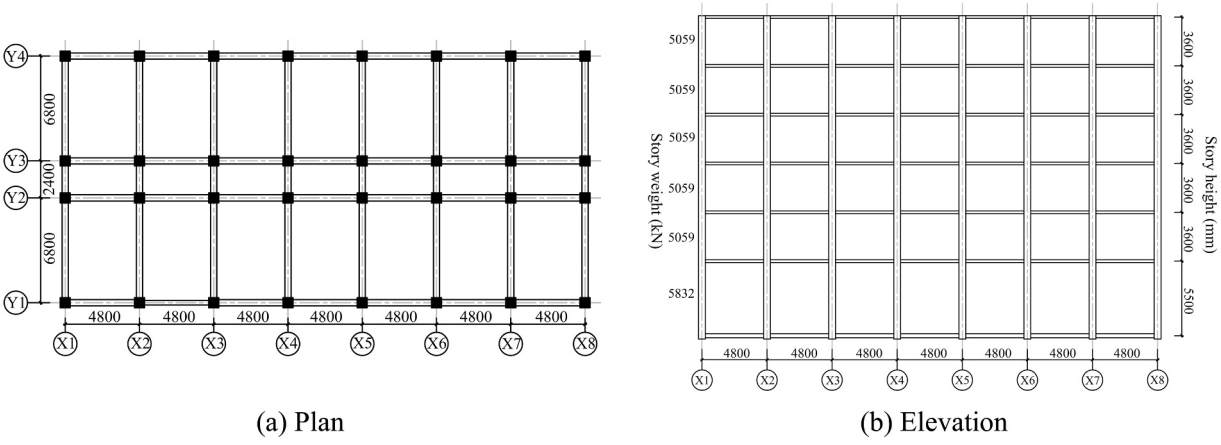

Fig. 7. Plan and elevation of the structure.

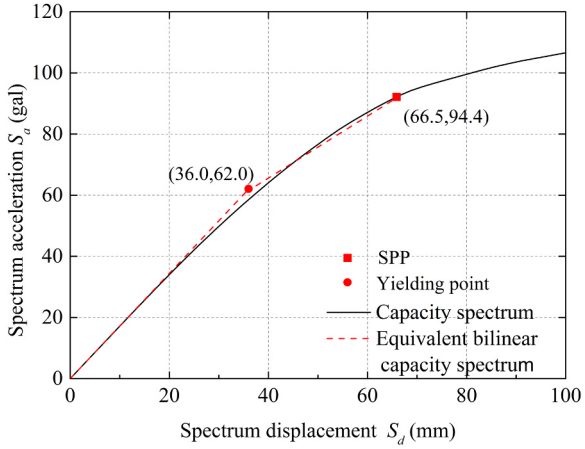

Fig. 8. Capacity spectra and SPP.

Table 6
Calculated results of the pushover analysis.

Story	Shear force Q_i (kN)	Story drift δ_i (rad)	Elastic stiffness K_{si} (kN/mm)	Target story drift $[\delta]$ (rad)	Displacement reduction ratio R'_{di}
1	3140	1/161	141	1/200	0.81
2	2670	1/158	170	1/200	0.79
3	2304	1/170	173	1/200	0.85
4	1928	1/214	171	1/200	1.07
5	1422	1/327	164	1/200	1.64
6	743	1/658	140	1/200	3.29

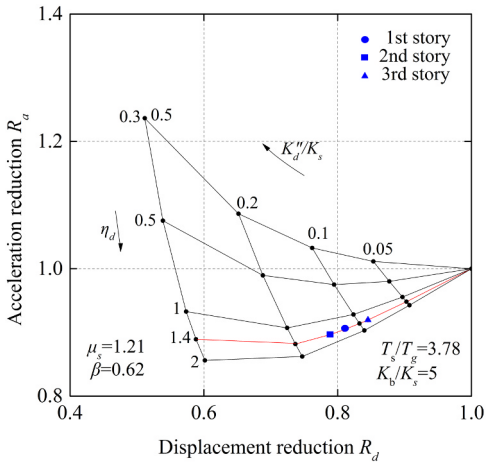

Fig. 9. EPRRCs for structure and story demand points.

Table 7
Total damping parameters of the VEDs.

Total parameters of the VEDs at each story	Story		
	1	2	3
Target displacement $[u_i]$ (mm)	27.5	18	18
Loss factor η_{di}	1.4	1.4	1.4
Loss stiffness ratio K''_{di}/K_{si}	0.12	0.14	0.09
Storage stiffness ratio K'_{di}/K_{si}	0.09	0.10	0.06
Storage stiffness K'_{di} (kN/mm)	12.69	17.00	10.38
Brace stiffness K_{bi} (kN/mm)	705	850	865
Damper displacement u_{di} (mm)	27.03	17.64	17.77
Maximum damping force F_{di} (kN)	590.12	515.95	317.32

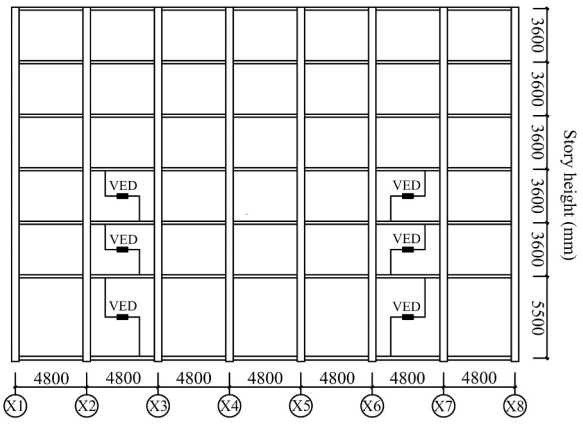

Fig. 10. Elevation of the VEDs arrangement on the Y1 and Y4 axes.

setting the $K_b/K_s = 5$, as shown in Fig. 9. In this study, the loss factor η_{di} of VEDs is set as 1.4, and then, the ratios of loss stiffness K''_{di}/K_{si} of VEDs installed at stories 1, 2 and 3 can be obtained according to η_{di} and R_{di} in the EPRRCs, as shown in Fig. 9. According to the aforementioned design procedure, the storage stiffness of the VED K'_{di}, the brace stiffness K_{bi} and the maximum damping force F_{di} are calculated as shown in Table 7, which shows that the calculated results satisfy the condition $K_{bi}/K''_{di} > 5$ recommended in the design procedure.

Four VEDs are needed for each story of the first three stories, and both frames on the Y1 and Y4 axes are arranged with the VEDs. The arrangements of the VEDs are shown in Fig. 10. The damping parameters of each VED are calculated as the total damping parameters divided by the number of dampers. Then, for convenience of the application, the calculated damping parameters of each VED are rounded up to suitable practical parameters, as listed in Table 8.

4.3. Verification

To verify the effectiveness of the design method, time history analysis is conducted on the structure with and without VEDs, which are denoted S0 and S1. Comparisons of the story drifts and story shear forces are performed between S0 and S1. In the time history analysis process, 10 different seismic waves are chosen according to the design response spectrum following Eq. (44) [51,52]. Among the 10 seismic waves, two of those (ASW1–2) are artificial seismic waves, and the others (NSW1-8) are natural seismic waves. The detailed information for the natural seismic waves is shown in Table 9. The design response spectrum and the response spectra of artificial seismic waves and natural seismic waves are presented in Fig. 11(a) and Fig. 11(b), respectively.

For different earthquake intensities, the peak ground accelerations (PGAs) of the abovementioned waves are 0.07 g for frequent earthquake, 0.2 g for moderate earthquake, and 0.4 g for severe earthquake. For PGA = 0.2 g, the time history analysis is performed using the S0 model. The calculated results and the target drift, which is 1/200 during a moderate earthquake as mentioned earlier, are presented in

Table 8
Practical parameters of each VED.

Practical parameters of each VED	Story		
	1	2	3
Number of dampers	4	4	4
Maximum damping force $F_{\max,i}$ (kN)	150	130	80
Storage stiffness K'_i (kN/mm)	3.5	4.5	3
Brace stiffness K_b (kN/mm)	180	220	220

Table 9
Seismic waves input information.

Name	Year	Event	Distance of epicentral (km)	Moment magnitude
NSW1	1942	Borrego	56.88	6.5
NSW2	1952	Kern County	38.42	7.4
NSW3	1971	San Fernando	22.77	6.6
NSW4	1971	San Fernando	39.45	6.6
NSW5	1976	Friuli_Italy-02	41.37	5.9
NSW6	1978	Tabas_Iran	24.07	7.4
NSW7	1979	Imperial Valley-06	35.64	6.5
NSW8	1980	Imperial Valley-06	15.84	5.8

Fig. 12. According to the average story drift of S0, the drifts of the 1st–3rd stories exceeded the target story drifts, and thus, the VEDs should be installed.

Next, time history analysis is performed on S0 and S1 under different earthquake levels. The average calculated results for different earthquake levels are compared to verify the response reduction effect, as shown in Figs. 13–15. The target story drifts for frequent and severe earthquakes are set to 1/550 and 1/80 according to the Chinese code, respectively [38]. As shown in Figs. 13–15, the maximum average story drifts of the structure are decreased from 1/443 to 1/563 for frequent earthquakes, from 1/167 to 1/205 for moderate earthquakes, and from 1/70 to 1/92 for severe earthquakes. All the target story drifts are satisfied for different earthquake levels. Additionally, the story shear forces are reduced due to the installation of VEDs. To check the energy dissipation effects, the hysteretic loops of the VEDs installed on the Y1 axis of the 1st–3rd stories are plotted in Fig. 16. The corresponding seismic wave is ASW1 for PGA = 0.2 g. According to the hysteretic loops, which are full, the VEDs show good energy dissipation capacity during a moderate earthquake.

5. Conclusion

In this paper, based on the EPRRC, a direct design method of VED parameters has been proposed by referring to the direct displacement-based design theory, which is the expansion of the method using the ERRC. To estimate the effects of the EPRRC, comparisons were made between the ERRC and the EPRRC. A benchmark six-story RC frame was illustrated adopting this proposed design method, and time history analysis was conducted to verify the effectiveness of this method. Thus, the following conclusions were obtained:

(1) The derived EPRRC can reflect the relationships between the VED parameters and the response reduction effect of the VED structural system in the elastic-plastic stage. The development of the EPRRC provides a more detailed theory for the design parameters of the VEDs of damped structures in the elastic-plastic stage.
(2) The traditional ERRC can overestimate response reduction of the VEDs, especially for acceleration reduction, whereas the EPRRC can estimate the response reduction of the VED structural system in the elastic-plastic stage, indicating that the design method based on the EPRRC is more reliable.
(3) Using the above-suggested design method, the displacement and shear force responses can be effectively reduced under different earthquake levels, and the story drift targets can also be satisfied as expected. Referring to the above discussion, it can be concluded that the proposed method is effective.

However, there are also some limitations to the proposed design method. The torsion irregularities and the flexural deformation of the primary structure were not considered in this study, in which only the shear stiffness of the primary structure was taken into account. These limitations are expected to be solved by upgrading the EPRRC to consider torsion irregularities and flexural deformation of the primary structure in future studies. Additionally, only the direction of the structure, which is the same as the direction of the pushover lateral force, is considered in the proposed design method. To consider every direction to install and design the damper, the 3D pushover may be adopted for the design of the VED parameters [53], which is expected to be examined in future analyses.

Acknowledgements

This study was supported by the National Natural Science Foundation of China under Grant nos. 51778489 and 51778490, the Shanghai Pujiang Program under Grant no. 17PJ1409200, the Fundamental Research Funds for the Central Universities under Grant no. 22120180064, the Key Program for International S&T Cooperation Projects of China under Grant no. 2016YFE0127600, the Sichuan Department of Science and Technology under Grant no. 2016JZ0009, and the Key Laboratory of Green Building in West China under Grant no. LSKF201804.

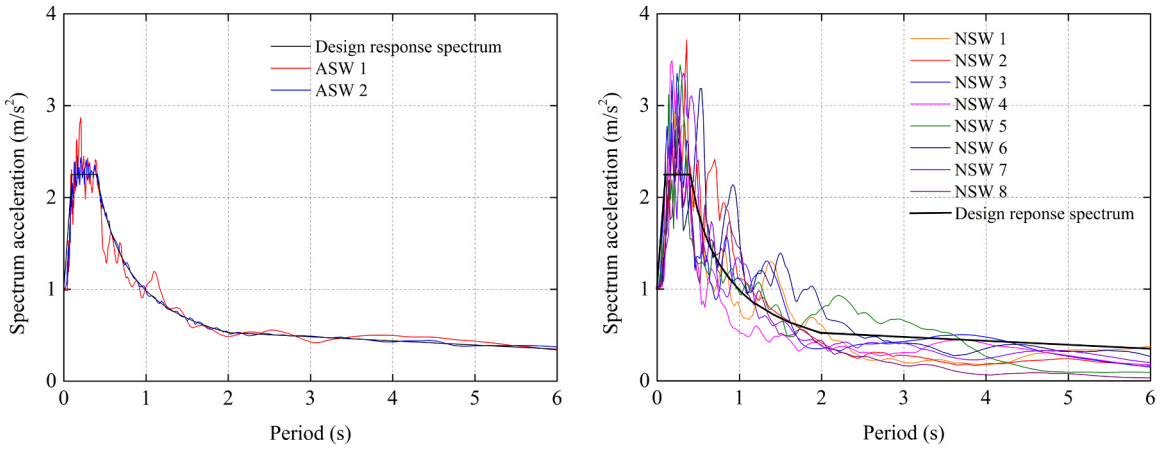

Fig. 11. Response spectra.

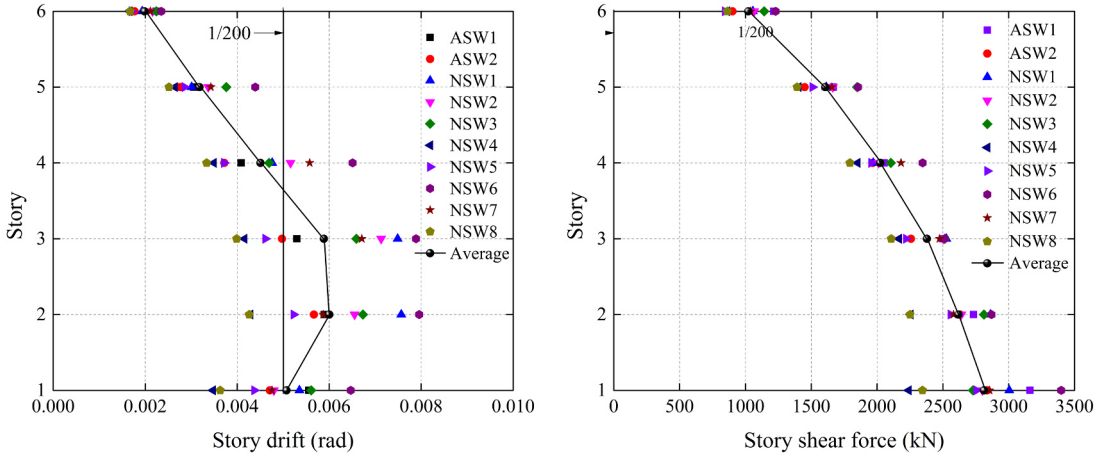

(a) Story drifts of S0 (b) Story shear forces of S0

Fig. 12. Seismic response for time history analysis (PGA = 0.2 g).

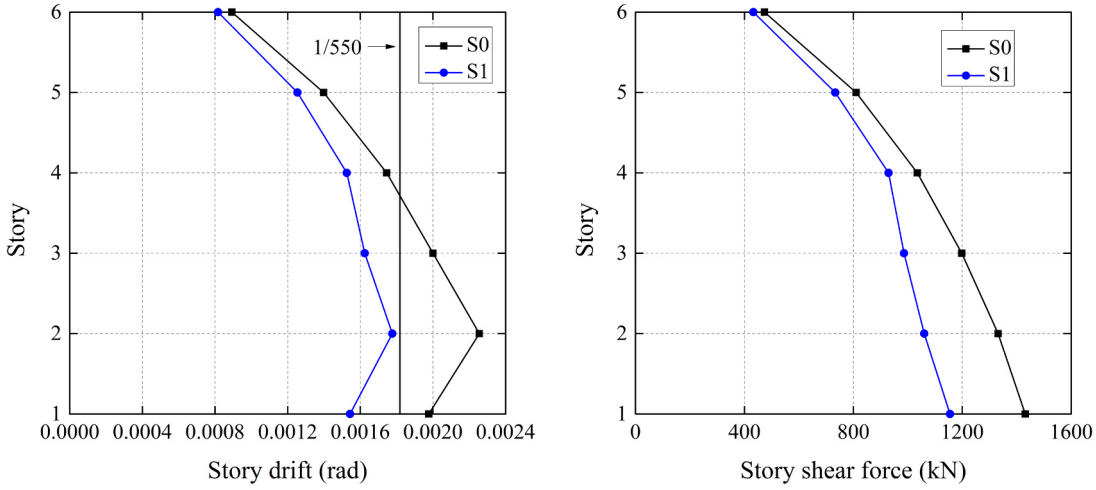

(a) Average story drift (b) Average story shear force

Fig. 13. Average seismic response for time history analysis (PGA = 0.07 g).

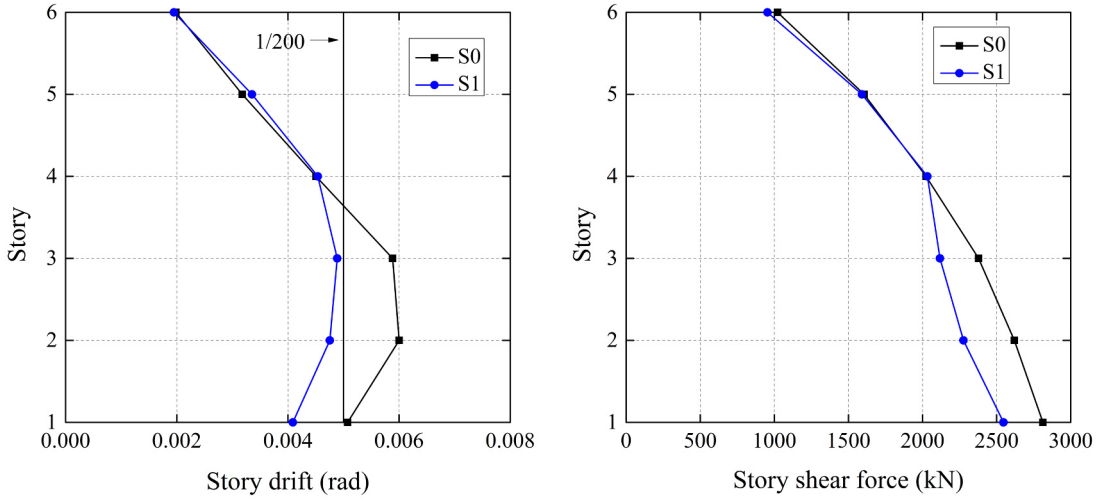

(a) Average story drift (b) Average story shear force

Fig. 14. Average seismic response for time history analysis (PGA = 0.2 g).

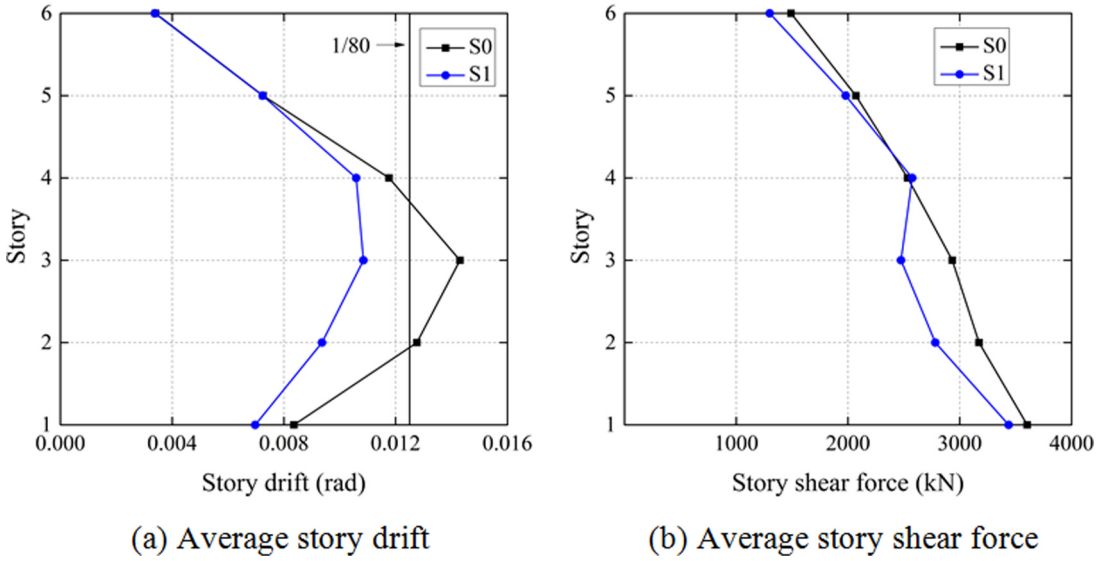

Fig. 15. Average seismic response for time history analysis (PGA = 0.4 g).

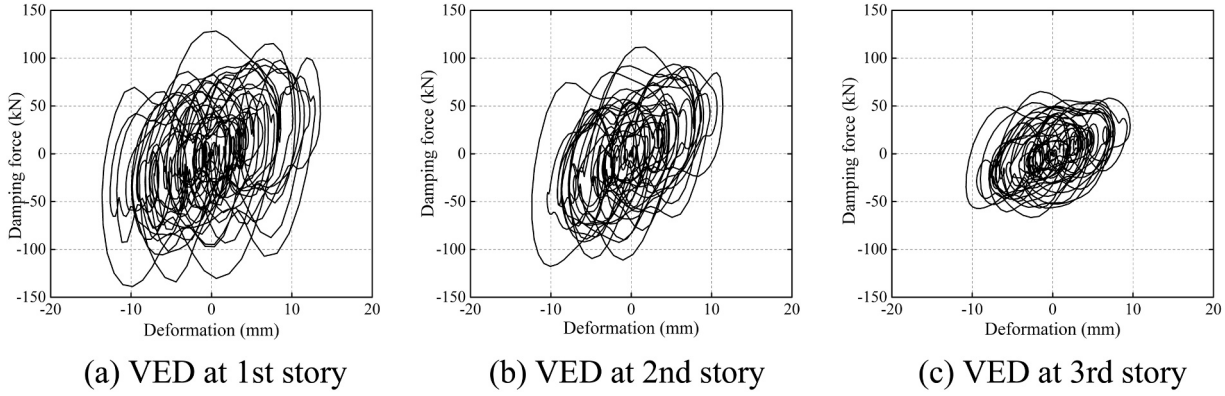

Fig. 16. Hysteretic loops of VEDs.

Appendix A. Detailed derivation of the damping ratios

With the aim of deriving EPRRC, the equivalent damping ratio ζ'_{eq} of the plastic-elastic VED structural system and of the primary structure without VED ζ^*_{eq} must be calculated. The added damping ratio of the VED ζ'_a and the effective damping ratio of the primary structure ζ'_s are two components of ζ'_{eq}, and the effective damping ratio ζ^*_s of the primary structure without VED is a part of ζ^*_{eq}. The derivation processes for these parameters are given as follows:

(1) According to the calculation diagram shown in Fig. A1, the derivation process of ζ'_a is given as follows:

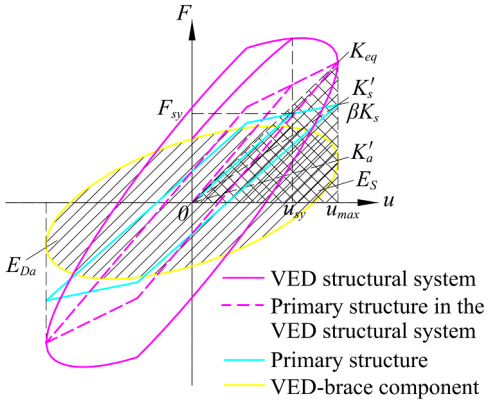

Fig. A1. Calculation of ζ'_a.

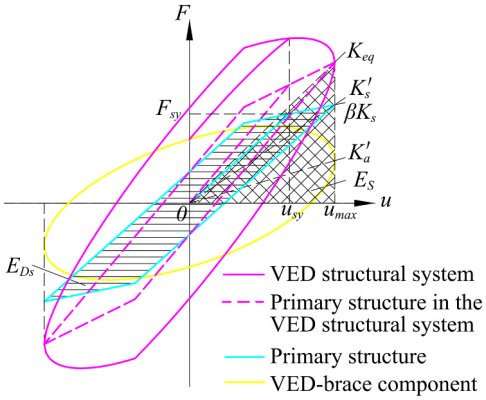

Fig. A2. Calculation of ζ_s'.

$$E_{Da} = \pi K_a'' u_{\max}^2 \tag{A1}$$

$$E_S = \frac{1}{2} u_{\max} [K_s u_{sy} + \beta K_s (u_{\max} - u_{sy}) + K'_a u_{\max}] \tag{A2}$$

$$\zeta_a' = \frac{E_{Da}}{4\pi E_S} = \frac{1}{2} \frac{\mu_s K_a''/K_s}{1 + \beta(\mu_s - 1) + \mu_s K_a'/K_s} \tag{A3}$$

where E_{Da} is the energy dissipated by the VED-brace component and E_S is the strain energy of the VED structural system.

(2) According to the calculation diagram shown in Fig. A2, the derivation process of ζ_a' is given as follows:

$$\begin{aligned} E_{Ds} = 4\{&[K_s u_{sy} + \beta K_s (u_{\max} - u_{sy})] u_{\max} - K_s u_{sy}^2 - \beta K_s (u_{\max} - u_{sy})^2 \\ &-2u_{sy} \beta K_s (u_{\max} - u_{sy})\} = 4K_s (1 - \beta) u_{sy} (u_{\max} - u_{sy}) \end{aligned} \tag{A4}$$

$$E_S = \frac{1}{2} u_{\max} [K_s u_{sy} + \beta K_s (u_{\max} - u_{sy}) + K_a' u_{\max}] \tag{A5}$$

$$\zeta_s' = \frac{E_{Ds}}{4\pi E_S} = \frac{2\rho(1 - \beta)(\mu_s - 1)}{\pi \mu_s [1 + \beta(\mu_s - 1) + \mu_s K_a'/K_s]} \tag{A6}$$

where E_{Ds} is the effective energy dissipation of the primary structure.

(3) According to the calculation diagram shown in Fig. A3, the derivation process of ζ_s^* is given as follows:

$$E_{Ds}^* = E_{Ds} = 4K_s (1 - \beta) u_{sy} (u_{\max} - u_{sy}) \tag{A7}$$

$$E_S^* = \frac{1}{2} u_{\max} [K_s u_{sy} + \beta K_s (u_{\max} - u_{sy})] \tag{A8}$$

$$\zeta_s^* = \frac{E_{Ds}^*}{4\pi E_S^*} = \frac{2\rho(1 - \beta)(\mu_s - 1)}{\pi \mu_s [1 + \beta \mu_s - \beta]} \tag{A9}$$

where E_{Ds}^* is the effective energy dissipation of the primary structure, and E_S^* is the strain energy of the primary structure without VED.

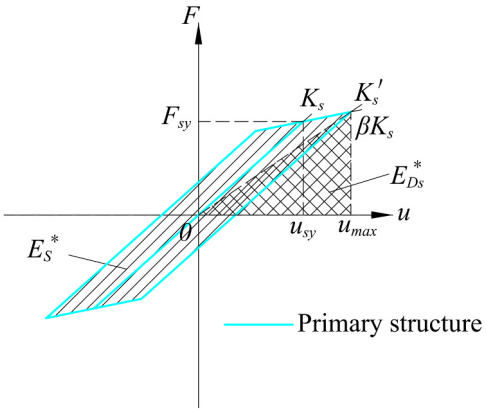

Fig. A3. Calculation of ζ_s^*.

References

[1] Soong TT, Dargush GF. Passive energy dissipation systems in structural engineering. London: Wiley; 1997.

[3] Pan C, Zhang RF. Design of structure with inerter system based on stochastic response mitigation ratio. Struct Control Health Monit 2018;25(6):e2169.https://doi.org/10.1002/stc.2169.

[2] Zhang RF, Zhao ZP, Pan C. Influence of mechanical layout of inerter systems on seismic mitigation of storage tanks. Soil Dynamics and Earthquake Engineering 2018;114:639–49. https://doi.org/10.1016/j.soildyn.2018.07.036.

[4] Chen QJ, Zhao ZP, Zhang RF, Pan C. Impact of soil–structure interaction on structures with inerter system. J Sound Vib 2018;433:1–15. https://doi.org/10.1016/j.jsv.2018.07.008.

[5] Rinaldin G, Amadio C, Fragiacomo M. Effects of seismic sequences on structures with hysteretic or damped dissipative behaviour. Soil Dyn Earthq Eng 2017;97:205–15. https://doi.org/10.1016/j.soildyn.2017.03.023.

[6] Kiris SS, Boduroglu MH. Earthquake parameters affecting the performance of an RC frame with friction damper. Soil Dyn Earthq Eng 2013;55:148–60. https://doi.org/10.1016/j.soildyn.2013.09.007.

[7] Hejazi F, Zabihi A, Jaafar MS. Development of elasto-plastic viscous damper finite element model for reinforced concrete frames. Soil Dyn Earthq Eng 2014;65:284–93. https://doi.org/10.1016/j.soildyn.2014.06.008.

[8] Pan C, Zhang RF, Luo H, Li C, Shen H. Demand-based optimal design of oscillator with parallel-layout viscous inerter damper. Struct Control Health Monit 2018;25(1):e2051.https://doi.org/10.1002/stc.2051.

[9] Luo H, Zhang RF, Weng DG. Mitigation of liquid sloshing in storage tanks by using a hybrid control method. Soil Dyn Earthq Eng 2016;90:183–95. https://doi.org/10.1016/j.soildyn.2016.08.037.

[10] Zhang RF, Wang C, Pan C, Shen H, Ge QZ, Zhang LQ. Simplified design of elasto-plastic structures with metallic yielding dampers based on the concept of uniform damping ratio. Eng Struct 2018;176:734–45. https://doi.org/10.1016/j.engstruct.2018.09.009.

[11] Symans MD, Charney FA, Whittaker AS, Constantinou MC, Kircher CA, Johnson MW, et al. Energy dissipation systems for seismic applications: current practice and recent developments. J Struct Eng 2008;134(1):3–21. https://doi.org/10.1061/(ASCE)0733-9445(2008)134:1(3).

[12] Mahmoodi P, Robertson L, Yontar M, Moy C, Feld L. Performance of viscoelastic dampers in world trade center towers. In: Proceedings of the Structures Congress. Orlando, FL: ASCE; 1987. p. 632–44.

[13] Kitagawa Y, Midorikawa M. Seismic isolation and passive response-control buildings in Japan. Smart Mater Struct 1998;7(5):581–7.

[14] Crosby P, Kelly J, Singh JP. Utilizing visco-elastic dampers in the seismic retrofit of a thirteen story steel framed building. In: Structures Congress XII. Atlanta, GA; 1994. p. 1286–91.

[15] Saidi I, Gad EF, Wilson JL, Haritos N. Development of passive viscoelastic damper to attenuate excessive floor vibrations. Eng Struct 2011;33(12):3317–28. https://doi.org/10.1016/j.engstruct.2011.05.017.

[16] Mazza F, Fiore M. Vibration control by damped braces of fire-damaged steel structures subjected to wind and seismic loads. Soil Dyn Earthq Eng 2016;83:53–8.

[17] Shen KL, Soong TT. Modeling of viscoelastic dampers for structural applications. J Eng Mech 1995;121(6):694–701. https://doi.org/10.1061/(ASCE)0733-9399(1995)121:6(694).

[18] Chang KC, Soong TT, Oh ST, Lai ML. Effect of ambient temperature on viscoelastically damped structure. J Struct Eng 1992;118(7):1955–73. https://doi.org/10.1061/(ASCE)0733-9445(1992)118:7(1955).

[19] Tsai C. Temperature effect of viscoelastic dampers during earthquakes. J Struct Eng 1994;120(2):394–409. https://doi.org/10.1061/(ASCE)0733-9445(1994)120:2(394).

[20] Xu ZD, Wang DX, Shi CF. Model, tests and application design for viscoelastic dampers. J Vib Control 2011;17(9):1359–70. https://doi.org/10.1177/1077546310373617.

[21] Lewandowski R, Pawlak Z. Response spectrum method for building structures with viscoelastic dampers described by fractional derivatives. Eng Struct 2018. https://doi.org/10.1016/j.engstruct.2018.01.041.

[22] Xu ZD, Xu C, Hu J. Equivalent fractional Kelvin model and experimental study on viscoelastic damper. J Vib Control 2015;21(13):2536–52. https://doi.org/10.1177/1077546313513604.

[23] Sun LM, Chen L. Free vibrations of a taut cable with a general viscoelastic damper modeled by fractional derivatives. J Sound Vib 2015;335:19–33. https://doi.org/10.1016/j.jsv.2014.09.016.

[24] Greco R, Marano GC. Identification of parameters of Maxwell and Kelvin–Voigt generalized models for fluid viscous dampers. J Vib Control 2015;21(2):260–74. https://doi.org/10.1177/1077546313487937.

[25] Lewandowski R, Pawlak Z. Dynamic analysis of frames with viscoelastic dampers modelled by rheological models with fractional derivatives. J Sound Vib 2011;330(5):923–36. https://doi.org/10.1016/j.jsv.2010.09.017.

[26] Lewandowski R, Chorazyczewski B. Identification of the parameters of the Kelvin-Voigt and the Maxwell fractional models, used to modeling of viscoelastic dampers. Comput Struct 2010;88(1–2):1–17. https://doi.org/10.1016/j.compstruc.2009.09.001.

[27] Palmeri A, Muscolino G. A numerical method for the time-domain dynamic analysis of buildings equipped with viscoelastic dampers. Struct Control Health Monit 2011;18(5):519–39. https://doi.org/10.1002/ stc.388.

[28] Aguirre M. Earthquake-resistant structure: structural frame damper system-an approach to design. In: Proceedings of the institution of civil engineers-structures and buildings; 1997. p. 165–72.

[29] Kim J, Choi H. Displacement-based design of supplemental dampers for seismic retrofit of a framed structure. J Struct Eng 2006;132(6):873–83. https://doi.org/10.1061/(ASCE)0733-9445(2006)132:6(873).

[30] Lin YY, Tsai MH, Hwang JS, Chang KC. Direct displacement-based design for building with passive energy dissipation systems. Eng Struct 2003;25(1):25–37. https://doi.org/10.1016/S0141-0296(02)00099-8.

[31] ATC-40. Seismic evaluation and retrofit of concrete buildings. Redwood City, CA: Applied Technology Council; 1996.

[32] Habibi A, Chan RWK, Albermani F. Energy-based design method for seismic retrofitting with passive energy dissipation systems. Eng Struct 2013;46:77–86. https://doi.org/10.1016/j.engstruct.2012.07.011.

[33] Tubaldi E, Barbato M, Dall'Asta A. Efficient approach for the reliability-based design of linear damping devices for seismicprotection of buildings. ASCE-ASME J Risk Uncertain Eng Syst, Part A: Civ Eng 2015;2(2). https://doi.org/10.1061/AJRUA6.0000858.

[34] Jensen NA, Sepulveda JG. On the reliability-based design of structures including passive energy dissipation systems. Struct Saf 2012;34(1):390–400. https://doi.org/10.1016/j.strusafe.2011.09.005.

[35] Zhang RH, Soong TT. Seismic design of viscoelastic dampers for structural applications. J Struct Eng 1992;118(5):1375–92. https://doi.org/10.1061/(ASCE)0733-9445(1992)118:5(1375).

[36] Heydarinouri H, Zahrai SM. Iterative step-by-step procedure for optimal placement and design of viscoelastic dampers to improve damping ratio. Struct Des Tall Spec Build 2017;26(9). https://doi.org/10.1002/tal.1361.

[37] Singh MP, Moreschi LM. Optimal seismic response control with dampers. Earthq Eng Struct Dyn 2001;30(4):553–72. https://doi.org/10.1002/eqe.23.

[38] Park KS, Koh HM, Hahm D. Integrated optimum design of viscoelastically damped structural systems. Eng Struct 2004;26(5):581–91. https://doi.org/10.1016/j.engstruct.2003.12.004.

[39] Manual JSSI. Design and construction manual for passively controlled buildings. Tokyo, Japan: Japan Society of Seismic Isolation(in Japanese); 2007.

[40] Hao LF, Zhang RF, Jin K. Direct design method based on seismic capacity redundancy for structures with metal yielding dampers. Earthq Eng Struct Dyn 2018;47(2):515–34. https://doi.org/10.1002/eqe.2977.

[41] Hao LF, Zhang RF. Structural safety redundancy-based design method for structure with viscous dampers. Struct Eng Mech 2016;59(5):821–40. https://doi.org/10.12989/sem.2016.59.5.821.

[42] Constantinou MC, Soong TT, Dargush GF. Passive energy dissipation systems for structural design and retrofit. Buffalo (NY): Research Foundation of the State University of New York and the Multidisciplinary Center for Earthquake Engineering Research; 1998.

[43] Fu YM, Kasai K. Comparative study of frames using viscoelastic and viscous dampers. J Struct Eng 1998;124(5):513–22. https://doi.org/10.1061/(ASCE)0733-9445(1998)124:5(513).

[44] Kasai K, Fu YM, Watanabe A. Passive control systems for seismic damage mitigation. J Struct Eng 1998;124(5):501–12. https://doi.org/10.1061/(ASCE)0733-9445(1998)124:5(501).

[45] Clough RW, Penzien J. Dynamics of structures. 2nd ed. New York: McGraw-Hill; 1993.

[46] GB 50011-2010. Code for seismic design of buildings. Beijing: The Ministry of Housing and Urban-Rural Construction of the People's Republic of China; 2010.

[47] Shen H, Zhang RF, Weng DG, Gao C, Luo H, Pan C. Simple design method of structure with metallic yielding dampers based on elastic–plastic response reduction curve. Eng Struct 2017;150:98–114. https://doi.org/10.1016/j.engstruct.2017.07.047.

[48] Computers and Structures, Inc.. Perform 3D, Nonlinear analysis and performance assessment for 3D structures, Version 5. Berkeley, CA: Computers and Structures, Inc.; 2011.

[49] GB 50010-2010. Code for design of concrete structures. Beijing: The Ministry of Housing and Urban-Rural Construction of the People's Republic of China; 2010.

[50] Takeda T. Reinforced concrete response to simulated earthquakes. J Struct Div Proc Am Soc Civil Eng 1970;96(12):2557–73.

[51] Pan C, Zhang RF, Luo H, Shen H. Target-based algorithm for baseline correction of inconsistent vibration signals. J Vib Control 2018;24(12):2562–75. https://doi.org/10.1177/1077546316689014.

[52] Pan C, Zhang RF, Luo H, Shen H. Baseline correction of vibration acceleration signals with inconsistent initial velocity and displacement. Adv Mech Eng 2016;8(10). https://doi.org/10.1177/1687814016675534.

[53] Reyes JC, Chopra AK. Three-dimensional modal pushover analysis of buildings subjected to two components of ground motion, including its evaluation for tall buildings. Earthq Eng Struct Dyn 2011;40(7):789–806. https://doi.org/10.1002/eqe.1060.